J Solid State Electrochem (2010) 14:549–553
DOI 10.1007/s10008-008-0654-8

ORIGINAL PAPER

Mechanism of lithium intercalation in titanates

Marina V. Koudriachova

Received: 30 May 2008 / Revised: 14 August 2008 / Accepted: 15 August 2008 / Published online: 6 September 2008

Abstract First principles calculations of Li insertion in a variety of titanate structures have revealed a common mechanism underlying the intercalation behavior of these materials. The mechanism is based on the accommodation of the electron density donated upon intercalation in particular orbitals of Ti ions and is governed by a strong coupling between the structural and electronic degrees of freedom. A new predictive model is developed which relates the local structure of TiO_2 polymorphs to their phase behavior upon Li intercalation.

Keywords Li battery · Anode material · Computer simulations

Introduction

Titanium dioxide is one of the few oxide materials that intercalates Li ions at low voltages and may be suitable as a battery anode. Titanium dioxide-based materials occur in a number of polymorphs, which exhibit a great variety in intercalation behavior. Some of them, in particular, Li titanates, have properties desirable for battery anodes including the reversible insertion of Li over a wide range of insertion concentrations at a constant potential, which is usually achieved through two-phase equilibrium between a Li-poor and a compatible Li-rich phase. Typically, single-phase (homogeneous) insertion results in a steadily declining discharge potential.

M. V. Koudriachova (✉)
Department of Chemistry, University College London,
Gower Street,
WC1E 6BT London, UK
e-mail: m.koudriachova@ucl.ac.uk

Li intercalation at a constant potential has been observed in the anatase- and spinel-structured Li titanates (at 1.8 eV [1] and 1.4–1.5 eV [2], respectively). The Li-rich phase for anatase was identified as an orthorhombic distortion of the parent tetragonal structure occurring at x=0.5 [3, 4] (x = [Li]/[Ti]) while the stable Li-rich phase of spinel-structured titanates adopts the cubic rock salt structure [5]. Among titanates that intercalate Li ions as a single phase are rutile (up to x=0.25) [1, 6–8], and the synthetic titanates with open channels—hollandite (TiO_2(H)) [9] and ramsdellite ((TiO_2(R)), up to x=0.5 [10], although there is still some controversy [11]. Recently, single-phase insertion to high Li concentrations was reported for nanostructured brookite [12]. Li insertion into rutile leads to a sequence of phase transformations [1, 6]. For x>0.25, the formation of a new phase was observed [1] and its structure identified with first principles calculations as a Li-rich monoclinic phase with x=0.75 [13]. Upon further lithiation, a monoclinic phase is predicted, which transforms irreversibly into a layered hexagonal phase degrading the electrode [1, 13]. In TiO_2(H) insertion above x>0.15 (as a single phase) is accompanied by a monoclinic distortion of the lattice [9]. Li insertion into TiO_2(R) at x>0.5 proceeds at a constant voltage (1.3 eV) [10], indicating a two-phase equilibrium with a Li-rich phase. Specially tailored nanostructures of the above polymorphs may allow for different intercalation behavior [14].

To direct a search for a material with improved intercalation properties, it is important to understand the relationship between its structure, morphology of its nanostructures, and the intercalation behavior. For TiO_2-based materials, this understanding is currently missing. The principal structural difference between different polymorphs resides in the lattice morphology, defined as the packing of the TiO_6 octahedra-sharing faces, edges, or

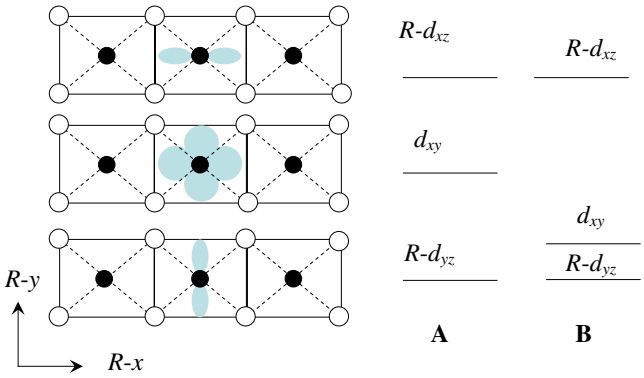

Fig. 1 Schematic representation of the ordering of the t_{2g}-derived orbitals (in *gray*) for TiO_2 polyhedra sharing two opposite edges. *A* rutile, *B* ramsdellite and hollandite. *Closed circles* denote Ti ions, *open circles* denote O ions. The *x*-axis is perpendicular to the picture

corners. Although the intercalation properties of titania have been studied extensively using a variety of experimental and theoretical techniques, the relationship between the insertion mechanism and the lattice morphology has not been established. The present study attempts to develop such understanding using first principles calculations and to build a conceptual framework to predict and rationalize the intercalation behavior of titanates. In this article, it is argued that accommodation of charge donated by inserted species to the lattice is the governing process in intercalation behavior. The structure/property relationship must, therefore, be based on an understanding of the coupling between electronic and structural degrees of freedom. First principles simulations have played an important role in developing an atomistic picture of the processes underlying Li insertion as they provide reliable thermodynamics and invaluable information on changes in electronic structure and local geometry [15–19]. In this study, first principles calculations form the basis for a simple and reliable model of intercalation behavior in titanates, which has been based on the analysis of more than 60 lowest energy configurations of various Li titanates for a wide range of Li insertion concentrations. The applications of the model presented in this study are exemplified by three study cases (rutile-, anatase-, and hollandite-structured TiO_2).

Details of calculations

Calculations were performed within the pseudopotential plane-wave formalism using the CASTEP software [20, 21]. Electron exchange and correlation effects were treated within the spin-polarized generalized-gradient approximation [22] with ultrasoft pseudopotentials used to replace the Ti (1*s*, 2*s*, 2*p*), O (1*s*), and Li (1*s*) core orbitals [23]. Reciprocal space was sampled on a regular net with a consistent spacing of 0.05 $Å^{-1}$. A plane-wave cut-off energy of 380 eV was found to converge the total energy to 0.01 eV per formula unit. Mechanical equilibrium was achieved by relaxation of the ionic positions and the size and shape of a computation unit through conjugate-gradient minimization of the total energy to an energy tolerance of 0.02 meV, and the forces are reduced to less than 0.05 eV/Å. The orbital hierarchy was obtained by analysis of the electron charge density using the Materials Studio software. Lowest energy configurations have been sought for a number of Li insertion concentrations. For each material, the lowest energy configurations at x=0.0625, 0.125, 0.1875, 0.25. 0.375, 0.4375, 0.5, 0.625, 0.75, 1 were sought using supercells representing various orderings of Li ions on the insertion sites. Local deformations were analyzed and the distribution of the charge donated upon intercalation was monitored. Supercells consisting of between one and eight primitive cells were used. Likely orderings of Li ions were explored using previous empirical Monte Carlo simulations [27] as well as analysis of local distortions at lower Li concentrations as described in [28]. The nature of the insertion process has been determined by comparing the thermodynamic stability of homogeneous and possible coexisting phases. Full details of this approach have been reported elsewhere [6].

Results and discussion

In titanates, the charge donated upon intercalation is distributed between the O and Ti ions. While extra charge on O ions leads to a volume expansion as the O ionic radius increases, the extra charge transferred to Ti ions is accommodated in the dt_{2g} derived states [24] at the bottom of the conduction band and potentially leads to a structural transformation. In an ideal TiO_6 octahedron, the t_{2g} states

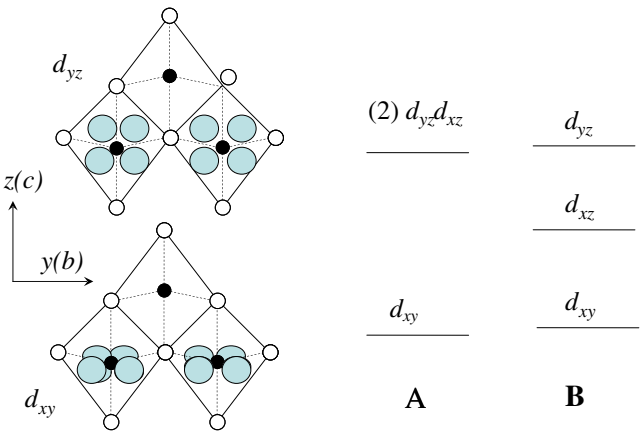

Fig. 2 Ordering of the t_{2g}-derived orbitals in polyhedra sharing two adjacent edges. *A* anatase, *B* brookite. The *x*-axis is perpendicular to the picture

Table 1 Edge sharing of TiO_6 octahedra and the t_{2g} states at the bottom of the conduction band of undoped titanates

Material	Shared edges				t_{2g} states
	Number	Opposite	Adjacent	Single	
Rutile	2	2	0	0	d_{yz}
Anatase	4	0	4	0	d_{xy}
Brookite	3	0	2	1	d_{xy}
Hollandite	4	2	2	0	d_{xy}/d_{yx}
Ramsdellite	4	2	2	0	d_{xy}/d_{yx}
Spinel $Li_{0.5}TiO_2$	6	6	0	0	Hybrid

The nature of the state is derived from the local geometry and confirmed by visual inspection of the occupied orbitals in undoped structures with one electron added

are degenerate. However, the degeneracy of these states is lifted by local distortions caused by the mutual repulsion of neighboring Ti^{4+} ions in octahedra connected across shared edges. As a result, O–Ti–O angles across the shared edges become more acute, while the adjacent angles become more obtuse. As the lowest energy t_{2g} states minimize repulsion with the valence charge density, their lobes point between the oxygen ions of the obtuse O–Ti–O angles, as shown in Figs. 1 and 2. In this way, the spatial orientation of the low-lying t_{2g} orbitals can be deduced directly from the geometry of the undoped structures (Table 1). Localization of the charge donated upon intercalation in these particular Ti t_{2g} orbitals leads to additional repulsions. The resulting structural deformations (derived from the spatial orientation of the occupied Ti t_{2g} orbitals) interact further with the orbital occupancy leading potentially to the orbitals degeneracy, which can be subsequently removed through a phase transformation. At high Li concentrations, accommodation of the donated charge in a single orbital becomes unfavorable as it results in the elongation of particular Ti–O bonds far beyond their equilibrium value. Instead, occupancy of fully hybridized orbitals is expected, corresponding to regular $Ti^{3+} - O_6^{2-}$ octahedra. When the induced distortions of the lattice create low-energy positions for additional Li ions, a cooperative distortion occurs, which leads to a stable Li-rich phase and two-phase intercalation.

A detailed examination of this mechanism is essential if intercalation in the various polymorphs is to be understood. The above model along with first principle calculations was applied to predict intercalation of Li ions into rutile-, anatase-, brookite-, ramsdellite-, and hollandite-structured TiO_2 and spinel-structured $Li_{0.5}TiO_2$. These form a representative set of TiO_2-based lattice morphologies. A polyhedral representation of these structures is shown in Fig. 3. The occupancy of the t_{2g} states upon Li insertion predicted by the model is compared with the computed occupancy in Table 2. There is an excellent agreement between intercalation behavior predicted by the model, the first principles

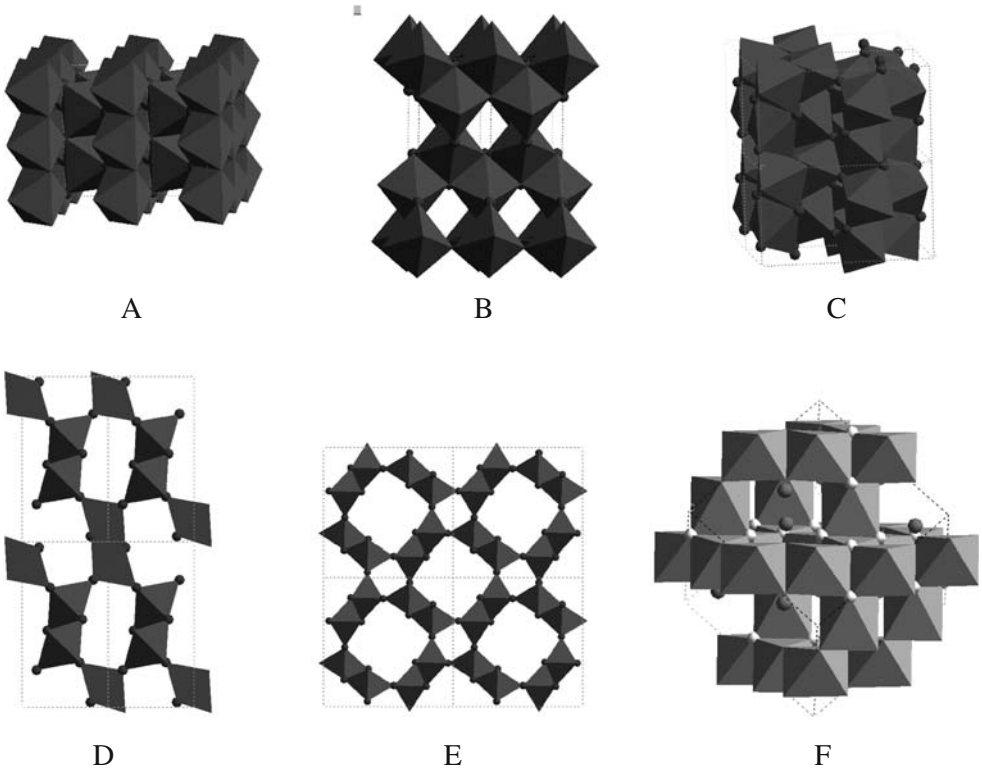

Fig. 3 Polyhedral representation of representative TiO_2 morphologies with the structure of rutile (**a**), anatase (**b**), brookite (**c**), ramsdellite (**d**), and hollandite (**e**) together with that of $Li_{0.5}TiO_2$ spinel (**f**)

Table 2 Occupancy of the orbitals predicted by the model from the geometry of the undoped structures and the concentration range of the lowest energy t_{2g}-derived states in Li-doped titanates obtained from first principle calculations

Material	Model	Calculations		
		d_{yz}	d_{xy}	d_{xz}
Rutile	$d_{yz}\rightarrow d_{xy}$	0.0625–0.25	0.75	–
Anatase	$d_{xy}\rightarrow d_{yz}\rightarrow$hybrid, x=1	0.0625–0.5	0.0625	–
Brookite	d_{yz}, d_{xy}, d_{xz}	0.0625–0.75	0.0625–0.75	0.0625–0.75
Hollandite	d_{yz}, d_{xy}	0.0625–0.75	0.0625–0.75	–
Ramsdellite	d_{yz}, $d_{xy}\rightarrow d_{xy}\rightarrow$hybrid, x=1	0.0625	0.0625–0.5	–
Spinel $Li_{0.5}TiO_2$	Hybrid	Hybrid		

calculations, and the experimental observations (Table 3). In what follows, the application of the above approach is illustrated using examples of rutile-, anatase-, and hollandite-structured TiO_2 where opposite, adjacent or both, opposite and adjacent, edges are shared, respectively. A full discussion of intercalation behavior of these and other titanate materials including detailed description of their lowest energy configurations and electronic structure at various Li concentrations is presented elsewhere (Koudriachova MV, in preparation) [25, 26].

For titanates with opposite edges shared (rutile), a Cartesian frame of reference is adopted in which a set of the shared opposite edges defines the *xy*-plane (Fig. 1). The deformation that occurs upon sharing of opposite edges makes the O–Ti–O angles across the shared edges more acute and the O–Ti–O angles adjacent to them more obtuse, so that the lowest energy orbital (d_{yz}) has its lobes pointing between the obtuse angles as shown in Fig. 1. Occupancy of the d_{yz} orbitals results primarily in the elongation of the O–Ti bonds along the *z*-direction and their tilting toward the *xy*-planes to restrict the volume expansion. These deformations accumulate with Li concentration, leading to occupancy of the d_{xy} orbitals alongside the d_{yz} orbitals. Due to repulsion with the valence charge density, upon occupancy of the d_{xy} orbitals, the smaller O–Ti–O angles in the *xy*-planes opens at the expense of the adjacent angles, reversing the stability of the d_{yz}/d_{xy} orbitals. For rutile, a single-phase insertion up to x=0.25 [6] (corresponding to the occupancy of d_{yz} orbitals) is followed by a two-phase equilibrium with the monoclinic x=0.75 phase [13] in which the d_{xy} orbitals are occupied. As discussed in [7], Li diffusion in rutile is highly anisotropic hindering homogeneous insertion, which is thus possible only at elevated temperature or in a nanophase.

Distortions associated with the sharing of adjacent edges (anatase) are discussed in a Cartesian frame of reference in which a set of shared adjacent edges defines the *yz*-plane (Fig. 2). The lowest energy orbitals (d_{xy}) are in the *xy*-planes where there is no edge sharing. These orbitals are shallow acceptor states as the corresponding Ti–O bonds are not coplanar. The deformations associated with occupancy of the d_{xy} orbitals include elongation of the Ti–O

Table 3 Intercalation behavior of various titanates predicted by the model in comparison with the results of first principle calculations and experimental data

Material	Model	Calculations, Li concentration		Constant potential, eV	
		1-phase	2-phases	Calc.	Exp.
Rutile	1 phase	0–0.25[a]			
	↓				
	2 phases		0–25–0.75	1.5	1.4[a] [1]
	↓				
	2 phases		0.75–1[b]		
Anatase	1 phase	0–0.0625			
	↓				
	2 phases	0.0625–0.75[a]	0.0625–0.75[a,c]	2.0	1.8 [1]
	↓				
	2 phases	0.75–1[a]	0.75–1[a]	1.6	1.6 [1]
Brookite	1 phase	0–1[a,d]	–	–	–
Hollandite	1 phase	0–0.75[d]	–	–	–
Ramsdellite	1 phase	0–0.5[d]			
	2 phases		0.5–1	1.28	1.34 [10]
Spinel, $Li_{0.5}TiO_2$	2 phases		0–0.5	1.5	1.38 [2]

[a] Elevated temperature
[b] Hexagonal phase
[c] Low temperature
[d] Sequence of single-phase insertion reactions

bonds in the z-direction, which is already longer than other bonds due to the crystal field splitting. Thus, at relatively low Li concentrations, occupancy of the orbitals at higher energies begins. In anatase, the d_{yz}/d_{xz} states are degenerate. Upon their occupancy (x=0.0625), the degeneracy is removed by a Jahn–Teller-like orthorhombic distortion of the lattice [4], which also creates new low-energy sites for Li ions. Thus, intercalation is expected to proceed via two-phase equilibrium. In the stable Li phase (orthorhombic $Li_{0.5}TiO_2$ [3, 4]) only d_{yz} orbitals are occupied, while the d_{xy} states are empty. At higher Li concentration, a regular geometry of TiO_6 octahedra corresponding to fully hybridized orbitals is expected, making new Li sites available. Consequently, a two-phase intercalation above x=0.75 and formation of $LiTiO_2$ rock salt phase [4] are predicted. Slow diffusion of Li ions out of the new sites is likely to be responsible for a quick ageing of anatase when intercalated to high Li concentrations [1, 7].

When both opposite and adjacent edges are shared, the d_{yz} and d_{xy} orbitals are nearly degenerate, so that their relative ordering is extremely sensitive to local distortions of the TiO_6 octahedra. In hollandite-structured TiO_2, these states do not become degenerate at any Li concentration as Li insertion into the large channels removes the structural equivalence of Ti ions: some Ti ions accommodate donated charge in the d_{xy} orbitals and others in the d_{yz} state. Therefore, at $0<x<0.5$, single-phase insertion is predicted with a monoclinic distortion of the lattice at $x>0.125$. As the insertion channels are large, fast diffusion and accessibility of the sites at room temperature are implied. Intercalation at $x>0.5$ is also predicted to proceed homogeneously as structural distortions of the open channels do not result in a new stable site for Li ions. However, at high Li concentrations, diffusion of Li ions is limited by their Coulombic repulsion, explaining the observed ageing of this material at $x>0.5$.

Conclusions

A systematic theoretical investigation of Li insertion into various TiO_2-based materials has been performed to pinpoint the mechanism underlying their intercalation behavior. Based on the computed results, a model that relates the intercalation behavior to the lattice morphology of the host material is suggested. The model is applied to rationalize intercalation behavior of various titanate structures. It is demonstrated that the intercalation behavior of these materials is dominated by a strong coupling between electronic and structural degrees of freedom and can be successfully predicted from their morphology. The model can be further applied to predict intercalation behavior of novel TiO_2-based structures, which can be synthesized in the nanophase.

References

1. Macklin WJ, Neat RJ (1992) Solid State Ion 53–56:694, doi:10.1016/0167-2738(92)90449-Y
2. Wang GX, Bradhurst DH, Dou SX, Liu HK (1999) J Power Sources 83:156, doi:10.1016/S0378-7753(99)00290-6
3. Cava RJ, Murphy DW, Zahurak S, Santorio A, Roth RS (1984) J Solid State Chem 53:64, doi:10.1016/0022-4596(84)90228-7
4. Koudriachova MV, Harrison NM, de Leeuw SW (2004) Phys Rev B 69:54106, doi:10.1103/PhysRevB.69.054106
5. Scharner S, Weppner W, Schmid-Beurmann P (1999) J Electrochem Soc 146:857, doi:10.1149/1.1391692
6. Koudriachova MV, Harrison NM, de Leeuw SW (2002) Phys Rev B 65:235423, doi:10.1103/PhysRevB.65.235423
7. Koudriachova MV, Harrison NM, de Leeuw SW (2001) Phys Rev Lett 86:1275, doi:10.1103/PhysRevLett.86.1275
8. Reddy MA, Kishore MS, Pralong V, Cainaert V, Varadaraju UV, Raveau B (2006) Electrochem Comm 8:1299
9. Noailles LD, Johnson CS, Vaughey JT, Tackerey MM (1999) J Power Sources 8182:259
10. Kuhn A, Amandi R, Garcia-Alvarado F (2001) J Power Sources 92:221
11. Gover RKB, Tolchard JR, Tukamoto H, Murai T, Irvine JTS (1999) J Electrochem Soc 146:4348
12. Reddy MA, Kishore MS, Pralong V, Varadaraju UV, Raveau B (2007) Electrochem Solid-State Lett 10:A29
13. Koudriachova MV, de Leeuw SW, Harrison NM (2003) Chem Phys Lett 371:150
14. Baudrin E, Caissaignon S, Koelsch M, Jolivet J-P, Tarascon J-M (2007) Electrochem Commun 9:337
15. Wolverton C, Zunger A (1998) Phys Rev Lett 81:606
16. van der Ven A, Aydinol MK, Ceder G, Kresse G, Hafner J (1998) Phys Rev B 58:2975
17. Mishra SK, Ceder G (1999) Phys Rev B 59:6120
18. Benedek R, Thackeray MM, Yang LH (1999) Phys Rev B 60:6355
19. Ceder G, Chiang Y-M, Sadoway DR, Aydinol MK, Jang Y-I, Huang B (1998) Nature 392:694
20. Payne MC, Teter MP, Allan DC, Arias TA, Joannopoulos JD (1992) Rev Mod Phys 64:1045
21. CASTEP 3.9 Academic version, licensed under the UKCP-MSI agreement
22. Perdew JP (1986) Phys Rev B 34:7406(E)
23. Vanderbilt D (1990) Phys Rev B 41:7892
24. Cotton FA, Wilkinson G, Gaus PL (1995) Basic inorganic chemistry, 3rd edn. Wiley, New York
25. Koudriachova MV (2008) Chem Phys Lett 458:108
26. Koudriachova MV (2008) Phys Chem Chem Phys 10:5094, doi:10.1039/b802421a
27. Kalikmanov VI, Koudriachova MV, de Leeuw SW (2000) Solid State Ion 136:1373
28. Koudriachova MV, Harrison NM, de Leeuw SW (2002) Comput Mater Sci 24:235